Color images visible under UV light

Roger D. Hersch, Philipp Donzé, Sylvain Chosson
Ecole Polytechnique Fédérale de Lausanne (EPFL)

Abstract

The present contribution aims at creating color images printed with fluorescent inks that are only visible under UV light. The considered fluorescent inks absorb light in the UV wavelength range and reemit part of it in the visible wavelength range. In contrast to normal color printing which relies on the spectral absorption of light by the inks, at low concentration fluorescent inks behave additively, i.e. their light emission spectra sum up. We first analyze to which extent different fluorescent inks can be superposed. Due to the quenching effect, at high concentrations of the fluorescent molecules, the fluorescent effect diminishes. With an ink-jet printer capable of printing pixels at reduced dot sizes, we reduce the concentration of the individual fluorescent inks and are able to create from the blue, red and greenish-yellow inks the new colorants white and magenta. In order to avoid quenching effects, we propose a color halftoning method relying on diagonally oriented pre-computed screen dots, which are printed side by side. For gamut mapping and color separation, we create a 3D representation of the fluorescent ink gamut in CIELAB space by predicting halftone fluorescent emission spectra according to the spectral Neugebauer model. Thanks to gamut mapping and juxtaposed halftoning, we create color images, which are invisible under daylight and have, under UV light, a high resemblance with the original images.

Keywords: Fluorescent ink images, fluorescent emission spectrum, spectral prediction model, juxtaposed halftoning, gamut mapping.

1 Introduction

Fluorescent inks visible under UV light but invisible under normal day light have long been used for the authentication of security documents, such as passports, bank notes, checks and vouchers (Van Renesse 2005). A single ink layer is used for printing either text or a monochrome image. Fluorescent inks are extensively used in the Euro bank notes, where both the stars and the silhouette of Europe are highlighted under UV light. Different fluorescent inks reemitting light at different wavelength ranges are starting to become available. We have found fluorescent inks for ink jet printers reemitting light in the blue, greenish-yellow and red wavelength ranges (www.riskreactor.com).

In the present contribution, we explore ways of creating color images invisible under day light and visible under UV light. Our aim is to obtain fluorescent images whose colors look similar to the colors of the original images from which they are derived.

RD.Hersch@epfl.ch, Sylvain.Chosson@gmail.com

Creating color images visible only under UV light raises a number of challenges. These challenges are (1) understanding the role of paper, (2) creating new colorants from a given set of fluorescent inks, (3) creating all colors within a color gamut by color halftoning, (4) establishing a color space for fluorescent emission spectra and performing gamut mapping from original image colors to the fluorescent inks' target gamut, and (5) performing the color separation from the mapped original colors to surface coverages of the fluorescent colorants.

The role of paper. Classical color separation and printing techniques rely on the fact that inks are printed on top of white paper. The white paper acts both as a colorant of its own (white) and as a reflector of the incoming light traversing a printed ink layer. Fluorescent inks absorb energy in the UV wavelength range and reemit part of the energy in the visible wavelength range. Paper acts as a support for depositing the ink and for reflecting the reemitted light upwards. Under UV illumination, non-printed paper areas are black (hereinafter: paper black). There is no paper white. The paper white needs to be replaced with a white colorant.

Creating new colorants from the available inks. In classical printing technologies, the superposition of solid cyan, magenta and yellow inks yields the new colorants red, green, blue and black. With fluorescent inks, can we create new colorants providing a significant extension of the fluorescent color gamut?

Halftoning with fluorescent inks. In classical clustered-dot color halftoning methods (e.g. the ones used for offset printing), the ink layers are halftoned independently from one another. Hence, the printed ink dots are partially superposed. Can we allow the fluorescent inks to be partially superposed? Is the resulting emission spectrum the sum of the emission spectra of each of the superposed inks? Or does the emission spectrum of one fluorescent ink reduce the emission spectrum of the other fluorescent ink? In such a case, what halftoning method should we adopt in order to avoid undesired superpositions of two fluorescent inks?

Color space for mapping original image colors to colors reproducible by fluorescent inks. In order to produce printed images visible under UV light which have a good resemblance with original color images, it is necessary to establish a common device-independent color space, e.g. the CIELAB space [Sharma 2003b; Wyszecki and Stiles 1982]. By performing gamut mapping in that color space, original colors shall be mapped into reproducible colors by introducing as few hue distortions as possible. Since there is no paper white, in order to convert from CIE-XYZ to CIELAB, what is the reference "white stimulus"?

Color separation from mapped original colors to surface coverages of the fluorescent inks. The classical color separation to cyan, magenta, yellow and black ink surface coverages is often performed by a look-up table. Such an approach requires printing hundreds of patches, measuring them and deriving by interpolation the entries of the look-up table [Bala 2003]. An alternative approach consists in establishing and calibrating a color prediction model which predicts the color produced with given surface coverages of the set of available colorants [Balasubramanian 1999; Stollnitz et al. 1998]. One may then fit the surface coverages of the colorants in order to produce a desired colorimetric value. This is the approach that we pursue in the present contribution.

Fluorescence. The fluorescence phenomenon is due to the transition of molecules from an excited state to a ground state. We consider molecules having two energy states, E_0 for the ground state and E_1 for the excited state [Nassau 1983]. When a molecule absorbs incident light, it is moved to one of the vibrational levels of the excited state E_1 (Figure 1, action A). The different vibrational states of an energy state correspond to the different vibrations between atoms within the molecule. Thanks to a non-radiative process, such as collisions leading to a small rise in temperature, a molecule at a high vibrational level v_i' of energy state E_1 falls back into the lowest vibrational level v_0' of energy state E_1. Then, in order to further release the absorbed energy and fall back into energetic ground state E_0, fluorescence will occur from vibrational level v_0' to the excited levels v_1, v_2, v_3 of the ground state (Figure 1, action F). The molecule will then return to its vibrational level v_0 by non-radiative transitions.
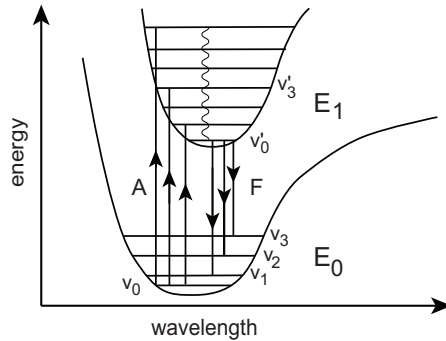
Figure 1: The energy levels of ground state E_0 and excited state E_1, with their corresponding vibrational states, and the transitions due to absorbance (A) and due to fluorescence (F).

We consider here fluorescent molecules which absorb in the ultraviolet wavelength range (320 nm - 380 nm) and reemit light in part of the visible wavelength range (380 nm - 730 nm). The spectrum of light emitted by fluorescence corresponds to the different changes of energy levels, from the vibrational state v_0' of excited state E_1 to the excited vibrational states of E_0. The shape of the spectrum emitted by fluorescence does not depend on the spectrum of the absorbed light [Emmel 2003, pp. 205-207]. Nevertheless, when the UV light source matches the absorption spectrum, the emitted spectrum has its highest relative intensity. At low concentrations of fluorescent molecules, the fluorescence phenomenon is approximately linear. However, at high concentrations, the behavior of the fluorescent substance is no longer linear: the absorption is too large, and temperature, dissolved oxygen and impurities reduce the quantum yield, i.e. the ratio between re-emitted photons and absorbed photons. This non-linear phenomenon is known as *quenching* [Nassau 1983].

In Section 2 we introduce related work such as a model of fluorescent inks visible under daylight and give an outline of our contributions. The measurement equipment setup is described in Section 3. In Section 4 we show the emission spectra of the inks and define the colorants that are used for printing the images visible under UV light. In Sections 5 and 6, we establish a spectral model for predicting the emission spectra of fluorescent ink halftones and derive a device independent color space for fluorescent inks. In Section 7 we describe a gamut mapping algorithm for mapping input colors into the reduced color gamut formed by the set of fluorescent inks. In Section 8 we describe the color separation and halftoning that is performed for printing color images visible only under UV light. In Section 9 we show the results and in Section 10 we draw the conclusions.

2   Related work

Fluorescent inks visible under daylight, such as the fluorescent ink present in yellow markers, have absorption components which absorb both in the UV and in the visible wavelength range and which contribute to the fluorescent emission at longer wavelengths. Such inks can be modeled by a fluorescence density matrix characterizing at each discrete wavelength the ink's absorption coefficient as well as its emission coefficient as function of the exciting wavelength [Emmel and Hersch 1998; Emmel 2003].

Monochrome invisible fluorescent inks are widely used in banknotes and security documents, for example for line art, microtext or pseudo-halftones. Specially conceived fluorescent security inks are able to emit different colors depending whether the illuminant is in the longwave ultraviolet range, i.e. around 365nm or in the shortwave ultraviolet range, i.e. around 254nm [Van Renesse 2005].

Coyle and Smith [2004] describe the use of red, green and blue emitting fluorescent inks for creating color images. Starting with an input cyan (*c*), magenta (*m*) and yellow (*y*) image, they deduce the corresponding surface coverages of red (*r*), green (*g*) and blue (*b*) by simple inversion, i.e. *r*=1−*c*, *g*=1−*m*, *b*=1−*y*. They propose to use the halftoning of standard ink-jet printers, generally error-diffusion or blue noise dithering. These halftoning methods rely on the superposition of the ink layers and may therefore yield quenching effects reducing the fluorescent emission spectra.

Narita and Eto [2002] describe how to create a thermal transfer sheet containing red, green and blue fluorescent inks, and how to transfer the inks onto paper by heating. They do not propose an explicit halftoning method and do not deal with the problem of reproducing an input color image.

Contributions. To our knowledge, there has not been a scientific approach for creating color images visible under UV light which preserve the original color image hues as much as possible.

We propose both a spectral model for predicting the emission spectra of fluorescent color images illuminated under a UV light source, and a method for converting the resulting emission spectra to the device-independent CIE-XYZ and CIELAB color spaces.

To reduce as much as possible quenching effects occurring when superposing fluorescent inks, we introduce the following approaches: Firstly, we create new colorants by superposing two or three inks at reduced pixel dot sizes. This is equivalent to a reduction of the concentration of the individual inks. Secondly, we propose a specially developed juxtaposed halftoning algorithm to ensure that colorants are printed side by side, with the paper black distributed between the colorant dots.

3   Measurement equipment, paper and printer

Standard desktop spectrophotometers only emit light in the visible wavelength range and are therefore inappropriate for measuring the emission spectrum of fluorescent materials. We created our own spectral measuring equipment by illuminating the print sample with collimated light from a Xenon light source (LINOS LQX-1000) filtered by a UV transmission filter (LINOS UG11). This yields a UV light emitting source in the range between 350 nm and 380 nm with a peak at 365 nm (Figure 2a).

The Xenon light source is connected to an optical fiber transmitting the light to collimating optics, from which the beam exits into the air and is filtered by the UV transmission filter, before reaching the printed paper at an angle of 45 degrees (Figure 2b). The reflected, respectively re-emitted light is captured perpendicularly to the print, by lenses focusing it into an optical fiber, which

brings it into an Oriel MS125 monochromator. The monochromator decomposes the incoming light into spectral components that are captured by photo-diodes converting light component intensities to electronic signals.
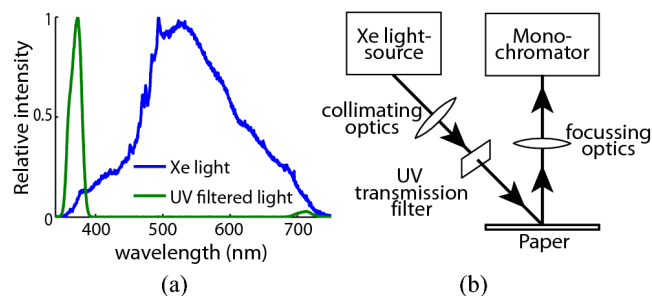

Figure 2: (a) Relative emission spectrum of the Xenon light source and the resulting filtered UV light spectrum. (b) Optical setup for measuring the emission spectra of patches printed with fluorescent inks.

Since the intensity of the light source slightly varies over time and since the sensitivity of the sensor also depends on the operating temperature, it is necessary to calibrate the measurement setup before carrying out spectral reflection measurements. When performing measurements in the visible wavelength light range, a perfectly white diffusing substrate such as Barium Sulfate ($BaSO_4$) is used as the reference white. However, in our case, the reemitted maximal fluorescence spectrum intensity is two orders of magnitudes lower than white light intensity. To obtain an acceptable dynamic range, we use as calibration patch a piece of dark gray paper which has a uniform reflectance spectrum.

Most "white" papers comprise fluorescent brighteners which emit light in the blue wavelength range. The strong blue-white light emitted by fluorescent paper tends to compromise the impact of the fluorescent ink emission. Therefore, we print the fluorescent inks on non-brightened papers, such as the "Biotop" 80 g/m^2 paper (www.mondibp.com).

Regarding fluorescent inks for color printing, we selected blue, red and greenish-yellow fluorescent inks from Risk Reactor. The printer is a Canon PIXMA iP4000 ink-jet printer working at an effective resolution of 600x600 dpi, offering 4 intensity levels: no dot, a small size dot (1 droplet), a middle size dot (2 droplets) and a large size dot (3 droplets).

4   Emission spectra of fluorescent inks

We carried out experiments in order to explore the colors visible under UV light that can be achieved by printing with the available set of fluorescent inks, and to test the possibility of establishing a spectral model predicting the emitted spectra as a function of the surface coverages of the individual inks. We were interested in (a) extending the color gamut by superposing two or three inks and (b) in creating intermediate colors within the gamut by juxtaposing (i.e. printing side-by-side) the inks and the new colorants formed by ink superpositions. We first measured the reflection spectra of each of the three available fluorescent inks (Figure 3).

The fluorescent inks absorb light in the UV wavelength range and reemit part of the light in the visible wavelength range. Therefore, within the visible wavelength range, the process is an additive process where colored light is emitted, rather than a subtractive process, where incident light is absorbed.

We verified that the fluorescence of the individual inks is linear with respect to the UV light source intensity by reducing its intensity, recalibrating the monochromator with the dark grey paper

reflector and measuring the emission spectrum. The relative departure from linearity is below 1% at 33% and below 4% at 12% of the UV light source intensity. For practical purposes, the single-ink fluorescent emission can therefore be considered as linear.
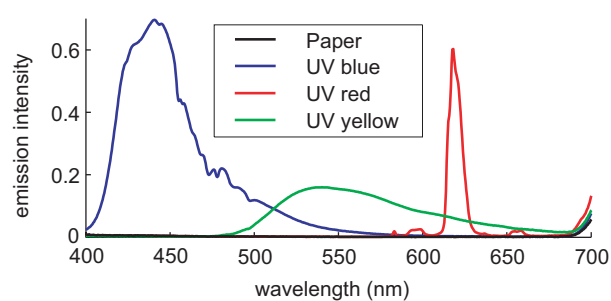

Figure 3: Emission spectra of the blue, red and greenish-yellow fluorescent inks.

In order to check if new colors can be obtained by superposing the solid inks, we created patches with all variants of two superposed solid inks. Figure 4 shows the emission spectra of the ink superposition patches illuminated under UV light.

Figure 4 indicates that the blue fluorescent ink dominates and considerably reduces the appearance to the second ink color. For example, the superposition of blue on red considerably reduces the intensity of the fluorescent red emission peak and, to some extent, also the intensity of the fluorescent blue emission spectrum.

We suspect that the predominance of the blue ink is due to the quenching effect, i.e. the blue ink has a high concentration of blue fluorescent molecules. Adding further potentially fluorescent molecules of the second ink creates a too high concentration limiting the fluorescence of the second ink's molecules.
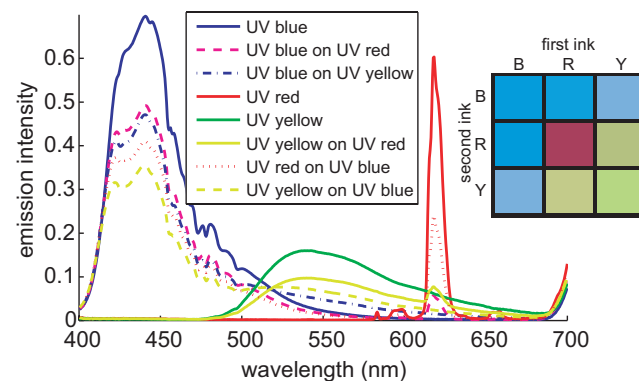

Figure 4: Spectra of patches printed with one or two superposed fluorescent inks and corresponding image.

Since the chosen ink-jet printer (Canon PIXMA iP4000) is able to print at three different droplet sizes, we can reduce the concentration of the blue ink by using medium dot sizes when blue is printed alone and small dot sizes when blue is superposed with another ink. In order to obtain a fluorescent color space incorporating the black-white axis, we need to create a fluorescent white colorant by appropriate superposition of the inks. We print all ink superpositions in all dot size combinations and select as white colorant the achromatic colorant having the most intense emission spectrum. The superposition variations of two inks yield the new colorant magenta, which considerably enlarges the fluorescent color gamut (Figure 8). The resulting set of colorants comprises blue (B: medium dot blue ink), red (R: medium dot red ink),

greenish-yellow (Y: medium dot greenish-yellow ink), magenta (M: small dot blue ink and large dot red ink), and white (W: small dot blue ink, medium dot red ink, and large dot greenish-yellow ink). The corresponding fluorescent emission spectra are shown in Figure 5.

In order to create color variations allowing to cover the color gamut given by the colorimetric values of the colorants and the paper black, we need to apply halftoning techniques. As shown in Figure 4, superposition of inks yields quenching, which reduces the corresponding ink emission spectra. Therefore, the fluorescent colorants should only be juxtaposed (printed side by side) and not superposed. Furthermore, in order to prevent undesired overlaps of colorants at the frontier between neighboring ink dots, the unprinted paper black space should be distributed between the fluorescent juxtaposed ink dots. The corresponding juxtaposed halftoning algorithm is described in Section 8.
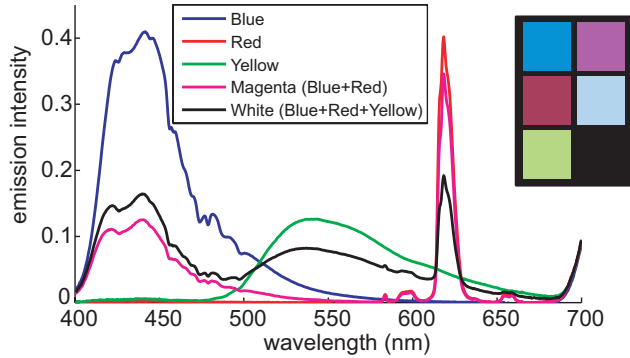

Figure 5: Fluorescent emission spectra of the blue, red, greenish-yellow, magenta and white colorants together with a photograph of the corresponding printed patches under UV illumination.

5   Spectral prediction model for fluorescent inks

We need to create a relationship between the surface coverages of juxtaposed fluorescent colorants and the color of the corresponding halftone when seen under UV light. In order to avoid measuring the emission spectra of hundreds of patches, we prefer to build a spectral model predicting the emission spectra as a function of the relative surface coverages of the contributing juxtaposed colorants.

For juxtaposed colorants, the simplest spectral prediction model is an adaptation of the spectral Neugebauer model [Neugebauer 1937; Viggiano 1990; Wyble and Berns 2000], which, in our case, predicts the fluorescent emission spectrum of a juxtaposition of m colorants of fluorescent emission spectra F_1, F_2, ... F_m of respective surface coverages u_1, u_2, ... u_m by

$$F(\lambda) = \sum_{i=1}^{m} u_i \cdot F_i(\lambda) \qquad (1)$$

It is known that the Neugebauer model does not take into account lateral propagation of light within the paper, nor internal Fresnel reflections at the print-air interface [Emmel 2003]. Therefore, in the case of normal prints, it does not provide accurate predictions.

In order to improve the prediction accuracy, Yule and Nielsen [1951] introduced a correction to the Neugebauer model in the form of a power function which, when applied to the spectral Neugebauer equations [Viggiano 1990], yields in the case of fluorescent inks the emission spectrum

$$F(\lambda) = \left(\sum_{i=1}^{m} u_i \cdot F_i^{1/n}(\lambda) \right)^{n} \qquad (2)$$

The scalar exponent n is fitted so as to minimize the sum of square differences between predicted and measured emission spectra components.

The surface coverages u_i that have to be used both in the case of the Neugebauer model (Eq. (1)) and in the case of the Yule-Nielsen model (Eq. (2)) should be the effective surface coverages, i.e. the surface coverages incorporating the dot gain [Bala 2003]. For both models, we create the curves mapping nominal to effective surface coverages by minimizing the sum of square differences between measured and predicted emission spectra components for nominal surface coverages values of 25%, 50% and 75% of each of the colorants (red, greenish-yellow, blue, magenta, white). Since the colorants are printed side by side and are as much as possible separated by unprinted space (paper black), we assume that the effective surface coverage of a colorant is independent of the surface coverage of the other colorants present in its neighborhood.

The nominal to effective surface coverage curves are shown in Figure 6. Clearly, the composed colorants magenta and white comprising two or respectively three superposed fluorescent inks have the largest dot gain.
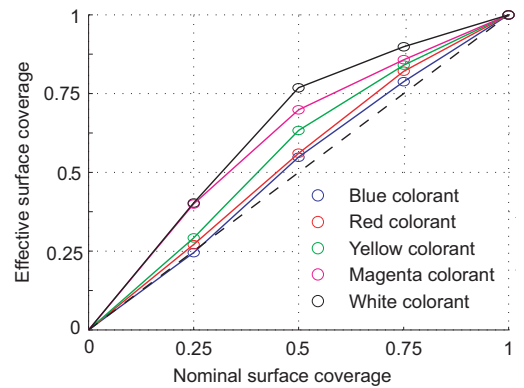

Figure 6: Nominal to effective surface coverage curves for the base colorants blue, greenish-yellow and red, and for the composed colorants magenta and white. Effective surface coverages are fitted by applying the Neugebauer model.

We evaluated the accuracy of both the spectral Neugebauer and the Yule-Nielsen model on 70 different representative fluorescent halftone test patches. Both the Neugebauer and the Yule-Nielsen models yield a mean prediction error of $\Delta E_{94}=3.5$. In the case of the Yule-Nielsen model, the optimal n-value is $n=0.92$, a value close to 1. The Yule-Nielsen model with a value of one is identical to the Neugebauer model. This indicates that lateral propagation of light within the paper and multiple internal reflections (Fresnel reflections) at the boundaries between the paper surface and the air do not have a significant impact on the emitted spectra.

This can be explained by the fact that emitted light propagating laterally is not absorbed by another ink. Indeed, since the presently used fluorescent inks are transparent in the visible wavelength range, they only emit light and do not absorb light. Only the paper absorbs a small fraction of the laterally propagating light. Therefore, once emitted from fluorescent ink molecules, light does not interfere with the light emitted from other fluorescent inks. As long as the individual inks are juxtaposed, we are in

the presence of a purely additive phenomenon, which is well modeled by the spectral Neugebauer equations.

Different commercial UV light sources may have different illuminant spectra. Since the shape of the spectrum emitted by a single fluorescent ink does not vary as a function of the absorption spectrum of the ink [Emmel 2003, p. 206], varying the UV illuminant only changes the relative intensity of the single ink emission spectrum. Our assumption, to be verified by experiments, is that the colorant spectra are modified according to the change of respective intensities of the contributing ink emission spectra.

6   A color space for fluorescent inks

In order to map original colors into the reduced gamut of the fluorescent inks, it is important to work within a device independent color space. Inspired by previous work on gamut mapping [Stone et al. 1988; Morovic 2003], we characterize the colors produced by fluorescent ink halftones in the widely used CIELAB color space. We first convert emitted spectra into tri-stimulus CIE-XYZ values [Sharma 2003b, p. 20] and then from CIE-XYZ to CIELAB [Sharma 2003b, pp. 29-31]. This conversion includes a normalization with respect to a "white stimulus", which simulates the eye's adaptation to lightness. When observing an image printed with fluorescent inks under UV light, we do not have a "white reference". We have the white colorant, whose maximal spectral intensity is approximately 2.5 times lower than the maximal spectral intensity of the fluorescent blue ink. We therefore adopt as pseudo white stimulus the spectrum of the white colorant, multiplied by this factor of 2.5.

With this procedure, we may now compare the gamut of our fluorescent inks with the gamut of standard sRGB monitor colors [Parulski and Spaulding 2003, pp. 749-751]. Figure 7 shows projections of the gamuts into the a^*b^*, L^*b^* and L^*a^* planes, respectively, as well as several constant lightness (L^*) slices. The boundaries of the set of printable fluorescent colors (shown in gray) are obtained by varying the relative surface coverages of the colorants. The colorant surface coverages are inserted into the spectral prediction model (Section 5) and the resulting emission spectra converted first into CIE-XYZ and then to CIELAB.
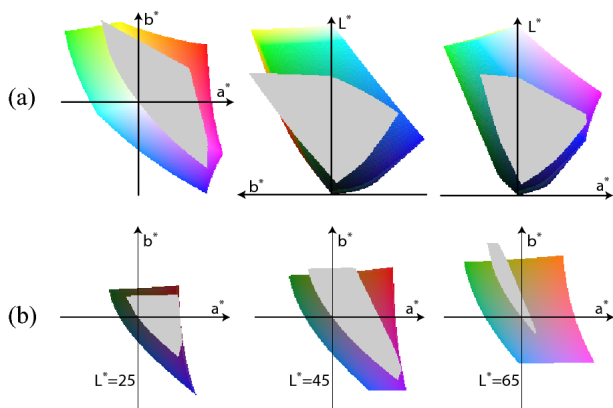

Figure 7: Gamuts of an sRGB monitor (colored) and of fluorescent ink halftones viewed under UV light (gray), (a) projected onto the a^*b^*, L^*b^* and L^*a^* planes and (b) shown as constant lightness slices.

Clearly, the part of fluorescent ink gamut (gray) in the 3rd quadrant (the green-blue color quadrant delimited by the -a and -b axes) is lacking, since there is no green fluorescent ink. Nevertheless, by performing an adequate gamut mapping step, we map the input colors into the reduced gamut of the fluorescent inks and try to obtain the best possible approximation of the input colors. Green-blue colors are mapped to gray, to desaturated greenish-yellow or to bluish colors.

7   Gamut mapping from a full color space to the reduced fluorescent color space

The present gamut mapping problem requires compressing the input gamut into the limited gamut offered by the fluorescent inks. The proposed mapping should preserve color continuity and whenever possible smoothness, i.e. a continuous color wedge located in the original color space should be mapped into a continuous color wedge located in the reduced target gamut. In addition, among different possible mappings, the mapping preserving at least to a certain extent the original hues is preferred.

The present gamut mapping problem has some resemblance with the problem of duo-tone printing. In both cases, a strategy needs to be adopted in order to map a "full" color gamut into a narrow color gamut located within a rather limited portion of the color space. In relationship with duotone printing, methods for gamut mapping have been proposed for the cases of one ink and black [Harrington 1992] and for two custom inks [Power et al. 1996]. These methods try to maintain overall relationships between colors by allowing strong hue shifts. For example, Power et al. [1996] try to map all hues into the hue range defined by the two custom inks.

Based on our experience of printing with custom inks visible under daylight [Chosson and Hersch 2002], we map in CIELAB space colors outside the available target gamut hues as desaturated "pseudo-gray" colors and colors inside the target gamut hues as close as possible to the original colors.

Let us first compute the gamut boundaries of the gamut formed by the fluorescent colorant emission. We establish in the CIE-XYZ color space a set of base tetrahedra whose vertices represent the colors of the fluorescent colorants and paper black. In order to avoid quenching, the colorants are separated one from another by as much paper black as possible. This yields a colorant separation scheme, where fluorescent colors are formed by white (W), black (K) and two chromatic colorants. Therefore, all base tetrahedra have in common the black-white axis [Ostromoukhov 1993]. For the presently selected set of inks and colorants, the black-white axis is located at the boundary of the gamut (Figure 7b, a*=0, b*=0). In the CIE-XYZ space, the resulting three adjacent base tetrahedra are formed by the colorants {K,W,B,M}, {K,W,M,R}, {K,W,R,Y}. Due to dot gain, the relationship between nominal colorant surface coverages and XYZ colorimetric values is not linear. The CIELAB space within which we would like to obtain the gamut boundaries and perform the color separation is also non-linear. For these reasons, we subdivide each base tetrahedron into 8 adjacent tetrahedra by creating a new vertex at each tetrahedron mid-edge point. By recursively performing this operation 4 times on each of the three base tetrahedra, we obtain a total of 12288 tetrahedra whose vertices represent the respective nominal surface coverages of the contributing colorants. Corresponding reflection spectra are predicted according to the Neugebauer model, converted first to CIE-XYZ and then to CIELAB. The set of all tetrahedra in CIELAB represents the target fluorescent ink emission gamut. External tetrahedra faces represent the gamut boundaries (Figure 8).

Each tetrahedron vertex represents a mapping between nominal surface coverages of the colorants and a CIELAB value. Since the tetrahedra are small, linear interpolation between tetrahedra vertices enables establishing the correspondence between CIELAB values and colorant surface coverages.

As in other gamut mapping methods [Morovic 2003], the first step in gamut mapping is to create a correspondence between the full lightness range (L^*=0 to L^*=100) and the fluorescent ink lightness range (paper black L^*=6.5 to white colorant L^*=69.5), by linearly scaling the lightness range of the fluorescent ink gamut.
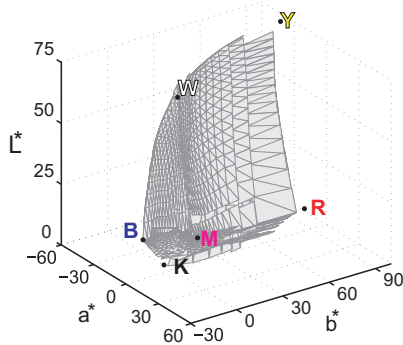

Figure 8: Gamut of the fluorescent inks in CIELAB space, represented by 12288 adjacent tetrahedra.

In order to map colors outside the available target gamut hues as desaturated "pseudo-gray" colors and colors inside the target gamut hues as close as possible to the original colors, we partition the color space into several parts along hue planes.

One hue plane is given by the hue of the solid greenish-yellow fluorescent colorant (Figure 9, H_Y) and the other by the hue of the solid blue fluorescent colorant (Figure 9, H_B). These two hue planes approximately delimit the domain A_{YB} of the hues present within the target fluorescent gamut. Its complement is the domain of hues outside the target gamut. Input colors located in that domain need to be projected into the target domain. For this purpose, we further partition the out of gamut hue domain into three parts, one part $A_{\perp Y}$ delimited by the yellow hue plane H_Y and by its perpendicular hue plane $H_{\perp Y}$ (Figure 9), the second part $A_{\perp B}$ delimited by the blue hue plane H_B and its perpendicular hue plane $H_{\perp B}$ (Figure 9) and the third part $A_{\perp Y \perp B}$ delimited by the hue half-planes $H_{\perp Y}$ and $H_{\perp B}$.
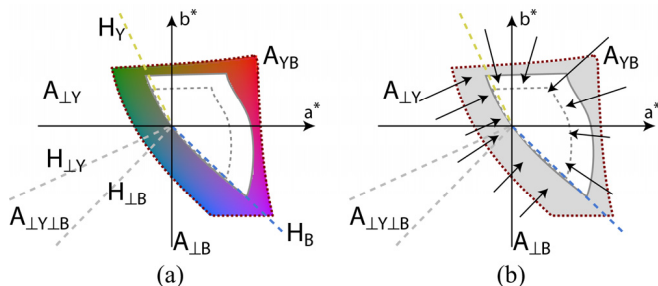

(a)   (b)

Figure 9: (a) Partition of the CIELAB color space into different hue domains. (b) Out of gamut color projection orientations.

We further define within the target gamut a core gamut boundary [MacDonald et al. 2000], which is a compressed instance of the target gamut boundary and which delimits a region of the color space that will be left unaltered. The target gamut "boundary volume" located between the target gamut and the core gamut is the space within which out of gamut colors as well as boundary volume colors are mapped. This mapping is linear, as shown in Figure 10a. Core gamut boundary points are obtained by projecting for a given lightness value the corresponding target boundary points perpendicularly towards the lightness axis. Input colors located within area A_{YB} are linearly mapped along their constant

lightness hue line into the target gamut boundary volume, as shown in Figure 10a.

Mapping of input colors located in out of gamut areas $A_{\perp Y}$ (Figure 10b) or respectively $A_{\perp B}$ of the input color gamut is performed by first projecting the colors perpendicularly towards the hue planes H_Y or respectively H_B, intersecting the projections with the target gamut boundaries (external tetrahedra faces) and by mapping the line segments located between input color gamut boundary and core gamut boundary into the target gamut boundary volume (Figure 10b). If there is no intersection with the target gamut boundary the color projected into the hue plane is further projected towards the black-white axis and mapped onto the resulting target gamut boundary intersection point. Input colors located in area $A_{\perp Y \perp B}$ are mapped by projecting them onto the black-white axis.
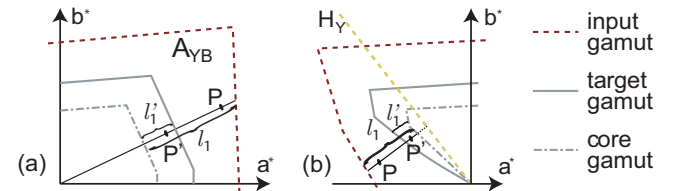

Figure 10: Mapping of constant lightness hue line segment l_1 into target gamut hue line segment l'_1 and of out of gamut color P into target gamut color P' in two different regions of the color space.

The presented gamut mapping method is also applicable to other sets of inks and colorants. The only condition is to have a white colorant located on the L^* axis. This is the case when the reference white stimulus (Section 6) is chosen as a scalar multiple of the white colorant.

8   Color separation and halftoning

After having performed the gamut mapping of an input color, color separating the mapped color consists of determining the respective amounts of the fluorescent colorants capable of reproducing that mapped input color, when viewed under UV light. The location of the mapped input color within the CIELAB space, i.e. its location within a tetrahedron, indicates which of the colorants and how much of them is necessary to create that color. Linear interpolation between tetrahedron vertices creates the correspondence between the mapped input color CIELAB value and the corresponding nominal surface coverages of the contributing colorant.

Once the nominal surface coverages of the contributing colorants are known, they are printed according to the same halftoning algorithm that is used to calibrate the spectral prediction model. In traditional color halftoning algorithms, the color screens are mutually rotated by 30 degrees and are partially overlapping [Hains et al. 2003]. In the present case, in order to avoid quenching which would reduce the fluorescent color gamut, we need a halftoning algorithm which avoids superposing fluorescent colorants, i.e. which does not yield overlapped screen dots. In addition, in case of dot gain and possible misregistration between the ink layers, screen dot overlaps should also be prevented. Juxtaposed halftoning, with colorant dots printed side by side and paper black surrounding them, meets these requirements.

The exact position of a screen element of one colorant depends on the amounts of the other colorants. For example, a surface coverage of $s_2 = 1/12$ of colorant c_2 is placed differently if the surface coverage of the neighboring colorant c_1 is small and that of c_3 is

large or vice-versa (Figure 11). The fact that the growing behavior of a colorant screen element depends on the neighboring colorant surface coverages excludes dither matrix based halftoning techniques.

(a) $s_1' = \frac{5}{12}$ $s_2' = \frac{1}{12}$ $s_3' = \frac{6}{12}$ (b) $s_3' = \frac{6}{12}$ $s_2' = \frac{1}{12}$ $s_3' = \frac{5}{12}$
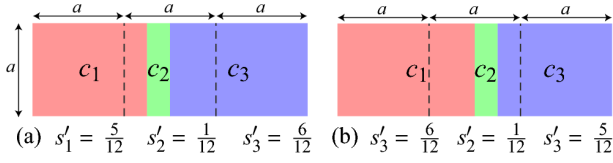
Figure 11: Colorant screen surfaces laid out horizontally according to their surface coverages.

We therefore create a library of screen element halftones incorporating all possible halftone combinations of 3 colorants c_1, c_2, c_3 and paper black c_4. We start by defining the base cells for a uniform distribution of colorants, i.e. $s_1 = s_2 = s_3 = 1/3$. Starting with square cells of side a, one may easily create a diagonally oriented screen with a 3x3 screen dot cell array, containing in one row the cells c_1, c_2 and c_3, and in each successive row the same cells, but shifted by one position (Figure 12). Such a 3x3 screen dot cell array has the advantage that a dot cell of a given colorant (e.g. c_1) has as its two direct horizontal neighbors and as its two direct vertical neighbors the two other colorants (e.g. c_2 and c_3).
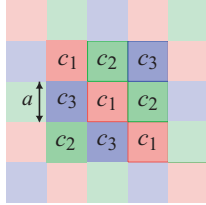

Figure 12: A 3 x 3 cell array, tiling the plane by horizontal and vertical replication.

To distribute the paper black evenly between colorant screen dots, we first compute from the initial distribution of colorant surface coverages s_1, s_2, s_3 a derived distribution s_1', s_2', s_3' covering the full screen surface without leaving holes. The unprinted surface part s_{paper} is evenly distributed among the colorants, i.e.

$$s_{paper} = 1 - s_1 - s_2 - s_3$$

$$s_1' = s_1 + \frac{s_{paper}}{3}, \ s_2' = s_2 + \frac{s_{paper}}{3}, \ s_3' = s_3 + \frac{s_{paper}}{3}$$

After having laid out the derived colorant surfaces, we will scale down each surface to $1 - s_{paper}$. This will ensure that the unprinted space is correctly placed around each colorant surface.

In order to generate clustered screen dots, we spread out the part of each colorant with surface coverage larger than 1/3 both horizontally and vertically into its neighboring dot cells in proportion to their unprinted surface coverage ratio (Figure 13). Figure 13a shows the case $s_1'>1/3$, $s_2'<1/3$, and $s_3'<1/3$, i.e. where the colorant surface ($s_1'-1/3$) is spread out over neighboring cells c_2 and c_3. Applying simple geometric considerations, we compute the width h of the horizontal and vertical bands allowing to distribute the surface $s_1'-1/3$ from cell c_1 into horizontal and vertical neighboring cells c_2 and c_3, according to the ratio of $1/3-s_2'$ and $1/3-s_3'$.

The equation system shown in Figure 13a comprises the surfaces s_{12}' and s_{13}' representing respectively the part of surface s_1' spilling out into cells c_2 and the part of it spilling out into cells c_3. Since the sum of the surfaces of three adjacent cells forms a unit surface, the corresponding nominal cell side is $a_n = \sqrt{1/3}$. In order

to obtain the band widths h_{12} and h_{13}, we solve this system of equations. Figure 13b shows the second case $s_1'>1/3$, $s_2'>1/3$, and $s_3'<1/3$, where respective surfaces of both c_1 and c_2 spill out into cells c_3. Again one solves the set of equations for the band widths h_{13} and h_{23}. We obtain well clustered screen dots.

After partitioning the screen element space according to the respective surface coverages s_1', s_2', s_3', the paper black is restored between the screen dots by scaling down each polygonal screen element shape so as to recover its original size. In order to create raster screen elements having a surface close to the surface of their respective polygons (polygons defining the surfaces s_1, s_2 and s_3), we need oblique polygon borders. The simple rasterization of rectangles with horizontal and vertical edges yields discrete surfaces whose size does not increase smoothly when slightly increasing their width or height. A slightly oblique square, e.g. a square having an angle of atan($1/m$), with $m \in Z$, yields rectangles of m different discrete sizes when translating one of its edge lines from zero to one unit in the x or respectively y direction. We therefore rotate the initial quadratic screen cells of side a forming the screen tile by a small angle (e.g. α=atan($1/a$)). We also scale them slightly (e.g. by $s = \sqrt{a^2+1}/a$) in order to have their vertices located on the grid. After having applied this transformation to all polygons of the screen tile, we rasterize them and obtain the screen element library entry associated with the desired fluorescent colorant surface coverages s_1, s_2, s_3 and the black coverage $s_{paper}=1-s_1-s_2-s_3$.

(a)
$$s_1' > \frac{1}{3}, \ s_2' < \frac{1}{3}, \ s_3' < \frac{1}{3}$$

$$s_{12}' = (s_1' - \frac{1}{3}) \frac{1/3 - s_2'}{2/3 - s_2' - s_3'}$$

$$s_{13}' = (s_1' - \frac{1}{3}) \frac{1/3 - s_3'}{2/3 - s_2' - s_3'}$$

$$w_2 = \sqrt{s_2'}; \ w3 = \sqrt{s_3'}$$
$$s_{12}' = (w_2 + \sqrt{1/3}) \cdot h_{12}$$
$$s_{13}' = (w_3 + \sqrt{1/3}) \cdot h_{13}$$
$$s_{23}' = 0$$

(b)
$$s_1' > \frac{1}{3}, \ s_2' > \frac{1}{3}, \ s_3' < \frac{1}{3}$$

$$s_{13}' = (s_1' - \frac{1}{3})$$

$$s_{23}' = (s_2' - \frac{1}{3})$$

$$w_3 = \sqrt{s_3'};$$
$$s_{13}' = (w_3 + \sqrt{1/3}) \cdot h_{13}$$
$$s_{23}' = (w_3 + \sqrt{1/3}) \cdot h_{23}$$
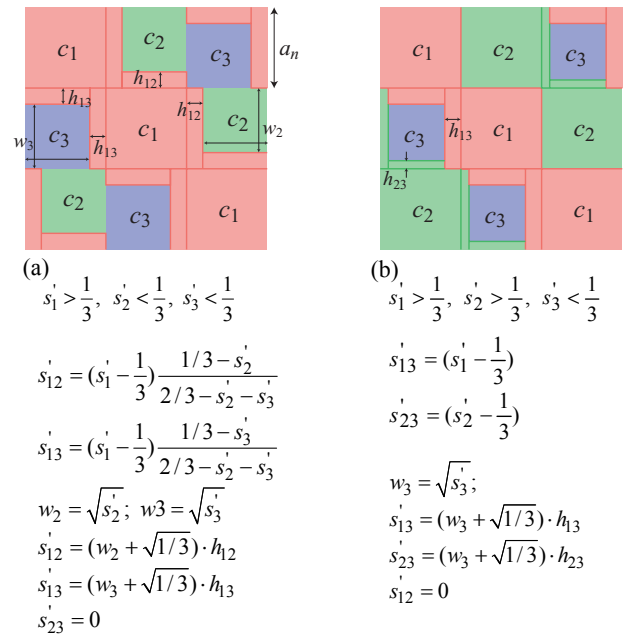$$s_{12}' = 0$$

Figure 13: Screen element surfaces growing both horizontally and vertically over neighboring cells, with (a) a single colorant c_1 growing over its two neighbors c_2 and c_3 and (b) the colorants c_1 and c_2 growing over their common neighbor c_3.

The screen element library with $n+1$ different intensity levels for a screen element surface size n is constructed by iterating for colorant c_1 over surface coverages s_1, from 0 to 1 in steps of $1/n$, for colorant c_2, by iterating over surface coverages from 0 up to the value of $1-s_1$, and for colorant s_3 from 0 up to the value of $1-s_1-s_2$ (constraint: $s_1+s_2+s_3 \leq 1$). According to Holladay [1980], one may represent an oblique screen element as a rectangular screen tile comprising the same number of pixels as the original obliquely oriented screen element, virtually replicated by a vector (t_x, t_y) so as to pave the plane. For a screen element hav-

ing 3 dot cells, with orientation $\alpha=\operatorname{atan}(1/a)$, the corresponding rectangular tile comprises $n=3(a^2+1)$ pixels. For example, a screen element of 3 dot cells, each having a surface of 65 pixels ($a=8$) yields a rectangular tile of size 195x1 pixels, with 3 bits per pixel for 5 colorants. By packing 8 pixels into 3 bytes, only 74 bytes per screen tile are needed. The corresponding screen element library requires a total memory size of 1'293'699 · 74 bytes ≈ 95.7 MB.

Once the screen element library is constructed, halftoning a color image simply consists of traversing the output image space scanline by scanline and pixel by pixel and then obtaining for each pixel the corresponding input image location and its source image color. One obtains the respective colorants and their surface coverages by accessing a previously established table providing the mapping between CIELAB colorimetric values and colorant surface coverages. The screen tile within the screen element library corresponding to the surface coverages s_1, s_2 and s_3 is accessed, and the colorant of the current pixel is read and copied to the current output image pixel.

Figure 14 shows a 2D color wedge halftoned according to the juxtaposed halftoning algorithm described above, using the colorants cyan, magenta and yellow and the paper white. Whenever possible, white space is surrounding each screen dot.
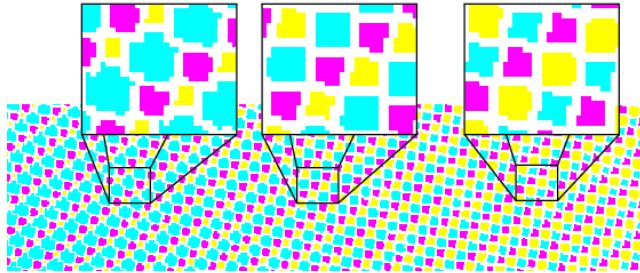

Figure 14: Simple 2D color wedge halftoned according to our juxtaposed halftoning algorithm (a=8), enlarged by a factor of 4.

9 Results

In order to demonstrate the effectiveness of the proposed approach without having to see the images under UV light, we simulate a fluorescent image by associating with each fluorescent colorant an RGB display color which yields "colorants" which look similar to the colorants visible under UV light. The "paper black" is simulated by standard black. Dot gain is simulated by applying a mathematical morphology dilation operation to the blue, red, greenish-yellow, magenta and white colorants and by introducing in the corresponding regions darkened instances of the original colorants.

Figure 15 shows uniform patches distributed over the CIELAB space. The original green patches are reproduced, due to the lack of a green fluorescent ink, by desaturated greenish-yellow patches. The cyan patches have desaturated bluish and black-white tones. The red part of the gamut is close to the original color. The brown patches have, due to gamut mapping, a reddish tone. In the frog image (Figure 16), the original hues are reproduced quite well.

In order to show the fluorescent images visible only under UV light in the proceedings, we printed the images in the illustration page with blue, red and greenish-yellow fluorescent offset inks having similar emission spectra as the corresponding ink-jet inks, but different superposition emission spectra due to a different quenching behavior. The colorant magenta is formed by the superposition of solid red and blue fluorescent inks and the colorant white by the superposition of solid blue, red and greenish yellow.
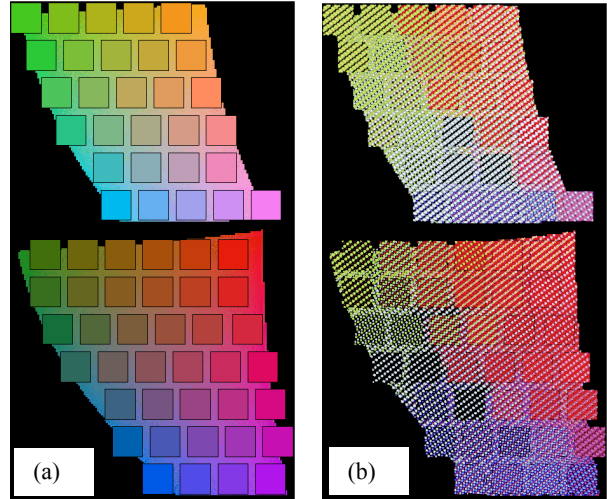

Figure 15: Uniform patches distributed over the CIELAB color space at lightnesses L*=*50* and L*=*70*. (a) Original sRGB image and (b) gamut reduced simulated fluorescent image viewed under UV light (halftone cell base a=8 pixels, at a resolution of 600dpi).
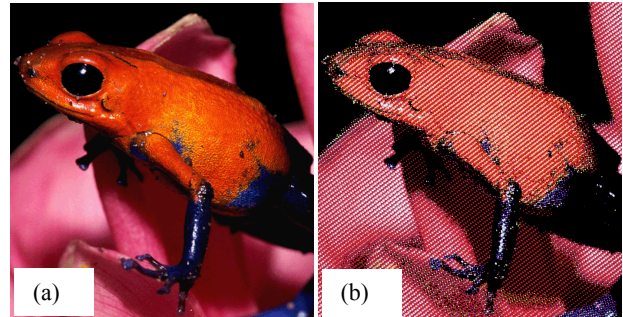

Figure 16: (a) Original sRGB image and (b) gamut reduced simulated fluorescent image viewed under UV light (same halftone parameters as in Figure 15).

10 Conclusions

We created a framework for reproducing color images with fluorescent inks. The considered fluorescent inks absorb energy in the UV wavelength range and reemit part of that energy in the visible wavelength range. Due to the quenching effect, when the concentration of the fluorescent molecules is too high, the fluorescent effect diminishes. By using a printer capable of printing pixels also at middle and small dot sizes, we are able to reduce the concentration of some of the inks and to create new colorants by superposing small, middle or large size dots of different inks.

Since light emitted by fluorescent juxtaposed colorants is primarily an additive process, the spectral Neugebauer model provides adequate predictions. We can therefore predict the emission spectra, and thus the CIELAB colors as a function of the surface coverages of the colorants. We map input image colors into the fluorescent color gamut, perform the color separations to obtain fluorescent colorant surface coverages and halftone them using juxtaposed halftoning.

The results show that colorful images visible only under UV light may be created with fluorescent inks emitting in different parts of the visible wavelength range. Even in the case where the fluorescent inks cover only part of the full color gamut, colorful consistent images may be produced.

Invisible fluorescent inks emitting in the red, green and blue wavelength ranges start to become available on the market. There-

fore, using at least one fluorescent ink having a color different from RGB is of high interest for the protection of security documents. The presented gamut mapping and juxtaposed halftoning techniques required to create color images with at least one non-RGB fluorescent ink make counterfeiting much more difficult. We intend to extend and optimize the presented techniques to fluorescent inks of various emission spectra, and possibly to images combining both classical and fluorescent inks.

Our primary application is the creation of color images for protecting security documents, such as ID cards, checks, vouchers or valuable business documents. Since the color images produced with fluorescent inks are only visible under UV light, they cannot be easily photocopied. Further applications are decorative applications, art, publicity, fashion, and night life, where digitally produced fluorescent images viewed under UV illumination at night or in the dark have a strongly appealing effect.

11 Acknowledgements

References

BALA, R. 2003. Device characterization. In Sharma (2003a), Ch. 5, 269–379.

BALASUBRAMANIAN, R. 1999. Optimization of the spectral Neugebauer model for printer characterization. *Journal of Electronic Imaging 8*, 2, 156–166.

CHOSSON, S. AND HERSCH, R.D. 2002. Color Gamut Reduction Techniques for Printing with Custom Inks, . In *Symposium on Electronic Imaging*, *SPIE* Vol. 4663, 110-120.

COYLE, W. J., AND SMITH, J. C. 2004. Methods and ink compositions for invisibly printed security images having multiple authentication features. US Patent Application 10/818,058.

EMMEL, P. AND HERSCH, R.D. 1998. Spectral Color Prediction Model for a Transparent Fluorescent Ink on Paper, *Proc. IS&T 6th Color Imaging Conf.*, 116-122

EMMEL, P. 2003. Physical models for color predictions. In Sharma (2003a), Ch. 3, 173–238.

HAINS, C., WANG, S.-G., AND KNOX, K. 2003. Device characterization. In Sharma (2003a), Ch. 6, 385–490.

HARRINGTON, S. J. 1992. Principles for mapping from full color to highlight color. In *Proc. of IS&T's 8th International Congress on Advances in Non-Impact Printing*, 459–462.

HOLLADAY, T. M. 1980. An optimum algorithm for halftone generation for displays and hard copies. In *Proceedings of SID*, Vol. 21, 185–192

HUNT, R. W. G. 1991. *Measuring Color*. Ellis Horwood, Chichester, England, p. 54.

MACDONALD, L. W., MOROVIC, J., AND XIAO, K. 2000. A topographic gamut mapping algorithm based on experimental observer data. In *Proceedings of 8th IS&T/SID Color Imaging Conference*, 311–317.

MOROVIC, J. 2003. Gamut mapping. In Sharma (2003a), Ch. 10, 639–685.

NARITA, S., AND ETO, K. 2002. Method for fluorescent image formation, print produced thereby and thermal transfer sheet thereof. US Patent US 7,005,166 B2.

NASSAU, K. 1983. *The Physics and Chemistry of Color*. John Wiley & Sons, New York City, NY, pp. 70 and 400-405.

NEUGEBAUER, H. E. 1937. Die theoretischen Grundlagen des Mehrfarbenbuchdrucks. vol. 36(4), 73–89. Reprinted in *Neugebauer Memorial Seminar on Color Reproduction*, *SPIE* Vol. 1184, 194–202.

OSTROMOUKHOV, V. 1993. Chromaticity gamut enhancement by heptatone multi-color printing. In *Symposium on Electronic Imaging*, *SPIE* Vol. 1909, 139–151.

PARULSKI, K., AND SPAULDING, K. 2003. Color image processing for digital cameras. In Sharma (2003a), Ch. 12, 727–757.

POWER, J. L., WEST, B. S., STOLLNITZ, E. J., AND SALESIN, D. H. 1996. Reproducing color images as duotones. In *Proceedings of ACM SIGGRAPH 96*, ACM Press, 237–248.

SHARMA, G., Ed. 2003a. *Digital Color Imaging Handbook*. CRC Press.

SHARMA, G. 2003b. Color fundamentals for digital imaging. In Sharma (2003a), Ch. 1, 1–114.

STOLLNITZ, E. J., OSTROMOUKHOV, V., AND SALESIN, D. H. 1998. Reproducing color images using custom inks. In *Proceedings of ACM SIGGRAPH '98*, ACM Press, 267–274.

STONE, M., COWAN W., BEATTY J. 1988. Color Gamut Mapping and the Printing of Digital Color Images, *ACM Transactions on Graphics*, Vol. 7, No. 3, Oct. 1988, 249–292.

TZENG, D.-Y., AND BERNS, R. S. 2000. Spectral-based six-color separation minimizing metamerism. In *Proceedings of the 8th IS&T/SID Color Imaging Conference*, 342–347.

VAN RENESSE, R. L. 2005. *Optical Document Security*. Artech House, London, 3rd edition, Chapter 4, Printing Inks and Printing Techniques, 97-127, Section on fluorescent inks, 98-104.

VIGGIANO, J. A. S. 1990. Modeling the color of multi-colored halftones. In *Proc. of the Technical Association of the Graphic Arts*, TAGA, 44–62.

WYBLE, D. R., AND BERNS, R. S. 2000. A Critical Review of Spectral Models Applied to Binary Color Printing. *Journal of Color Research and Application* Vol. 25, No. 1, 4–19.

WYSZECKI G. AND STILES W.S.,1982, *Color Science*, 2nd Ed., Wiley.

YULE, J. A. C., AND NIELSEN, W. J. 1951. The penetration of light into paper and its effect on halftone reproduction. In *Proceedings of the Technical Association of the Graphic Arts*, TAGA, vol. 3, 65–76.

Illustrations : Fluorescent color images to be viewed under UV light

Color images visible under UV light

Printed in offset by
Perfect SA
Etoy, Switzerland
www.perfect.ch

Technical specifications:
Resolution: 1200 dpi
Halftone cell base a=8 pixels

Figure A1: Ski equipment, visible under UV light.

Figure A2: Fruits, visible under UV light.

Figure A3: Frog, visible under UV light.

Figure A4: Tiger, visible under UV light.

Figure A5: Butterfly, visible under UV light.